INVESTIGATION OF NATURAL PERMEABILITY IN GRABEN SYSTEMS: SOULTZ EGS SITE (FRANCE)

P. Baillieux[1], E. Schill[1], L. Moresi[2], Y. Abdelfettah[1], C. Dezayes[3]

[1]Centre for Hydrogeology and Geothermics,
Neuchâtel University, Rue Emile Argand 11,
CH-2009 Neuchâtel, Switzerland

[2]School of Mathematical Sciences,
Monash University, Wellington Rd
Clayton 3800 VIC, Australia

[3]BRGM (French Geological Survey)
3, avenue Claude Guillemin,
BP36009, F-45060 Orléans Cedex 2, France

e-mail: paul.baillieux@unine.ch

ABSTRACT

Two different approaches have been employed to investigate the localization of fault zones and natural permeability at regional and local levels in extensional tectonic settings with potential for EGS technology.

Regional distribution of potential permeable fault zones has been analyzed dynamically using a new 2D geodynamic model. Numerical simulation of instability of a viscoelastic-plastic lithosphere require a lower crustal viscosity in the order of $5 \cdot 10^{21}$ to 10^{22} Pa s to match the deformation pattern of the Upper Rhine Graben (URG). Models clearly show a localization of deformation at regional level, but do not explain the internal fault distribution on the horst level as it can be seen at the Soultz. This has been investigated further using geophysical means.

The high-resolution 3D structural regional model of the Soultz area is used as a basis for new geophysical interpretation and inversion of gravimetric and magnetic data. Several gravimetric and magnetic anomalies can be linked to thermal anomalies, which in general the Upper Rhine Graben are known to be linked to free convection and thus, linked to porosity and permeability changes.

INTRODUCTION

The URG reveals several heat flow anomalies in the order of up to > 160 mW m^{-2}. One of those at Soultz-sous-Forêts has been selected to develop the Hot Dry Rock technology in 1987. Given the occurrence of natural fractures and hydrothermal fluid in the subsurface, the project has been developed using Enhanced Geothermal System (EGS) technology and is today the only EGS project under exploitation world-wide. The enhanced surface heat flux in the Upper Rhine valley has been related to the circulation of thermal water along fault zones (Illies 1965). Numerical simulation of the neighboring geothermal site of Landau have confirmed this hypothesis (Bachler *et al.* 2003).

Localization of geothermal highs in the URG can be observed at two different levels. At a region scale for example, these are found in the North Western part of the graben (Fig. 1), in the part which is opposed to the major deformation accommodated by the Eastern master fault (Mauthe *et al.* 1993). At a local scale, the example of the Enhanced Geothermal System (EGS) site Soultz is found to be located in the northern part of a horst structure. Within this horst, the thermal anomaly localizes between the Soultz and Kutzenhausen faults only at its western edge (Baillieux *et al.* 2011).

Other recent studies highlighted the link between temperature anomaly and its state of fracturing at Soultz: a thermo-hydraulic simulation around the geothermal wells predicts fluid convection with permeability up to 3×10^{-14} m^2 in these strongly fractured zones (Kohl *et al.* 2000). The low resistivity anomaly at the western part of the horst in the

magnetotelluric inversion is interpreted to be the presence of clay minerals, due to hydrothermal alteration of granite or by the presence of the saline brine by itself (Geiermann and Schill 2010). A density anomaly of about 250 kg.m^{-3} has been observed in the granitic basement below the Soultz site on the 3D inversion of existing gravity data in combination with a previous geological model (Schill *et al.* 2010). It has been attributed to an increase in porosity due to strong fracturation and the presence of leucogranitic bodies in this structure, supported by geological observations in the wells EPS1 and GPK1 (Genter *et al.* 1995).

In this study, we aim at understanding the formation and localization of fracturing in graben systems using an integrated approach:

First, we use graben-wide seismic sections (Brun *et al.* 1992) (see Fig.2 and their location in Fig.1) and geological knowledge of the well-studied URG as an ideal database for benchmarking geodynamic models of crustal extension at a regional level, allowing the visualization of formation of faulted zones through time.

Secondly, our high-resolution 3D structural regional model (Baillieux *et al.* 2011) (location in Fig. 1) is used as a basis for new geophysical interpretation and inversion of gravimetric and magnetic data. These are used for re-interpretation of the geophysical anomalies.

KEY TECTONIC INFORMATION ON THE UPPER RHINE GRABEN

The Upper Rhine Graben (URG) is a central segment of the European Cenozoic Rift System (ECRIS) and originates from the Alpine and Pyrenean collisions (Ziegler 1992). It represents a typical example of syn-orogenic, intra-continental foreland rifting (Schumacher 2002; Dèzes *et al.* 2004; Cloetingh *et al.* 2010). This rifting is related to foreland indenter effects and ensuing escape tectonics: lithospheric over-thickening in orogenic belts, resulting in uplift and extension of their axial part. The main rifting stage of the URG formation was an E-W extension taking place from the end of the Oligocene to that of the Eocene (Villemin and Bergerat 1987). Inherited Variscan tectonic structures have a strong impact on the localization of deformation up to recent times (Schumacher 2002; Edel *et al.* 2006).
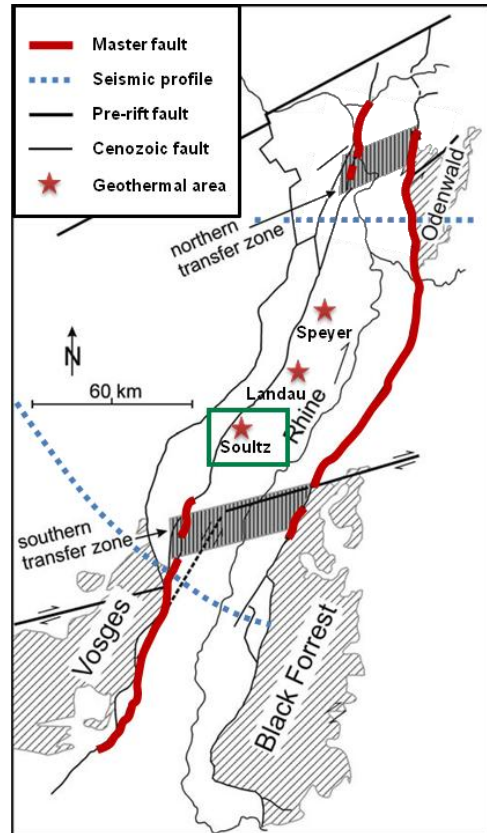

Figure 1: Structural interpretation of the Upper Rhine Graben. Red lines denote the spatial distribution of the graben master faults. Blue dashed lines show the location of the ECORS-DEKORP seismic lines. Red stars show the main geothermal anomalies of the upper Rhine Graben.Green rectangle shows the geological model location. Modified after Derer et al. (2005).
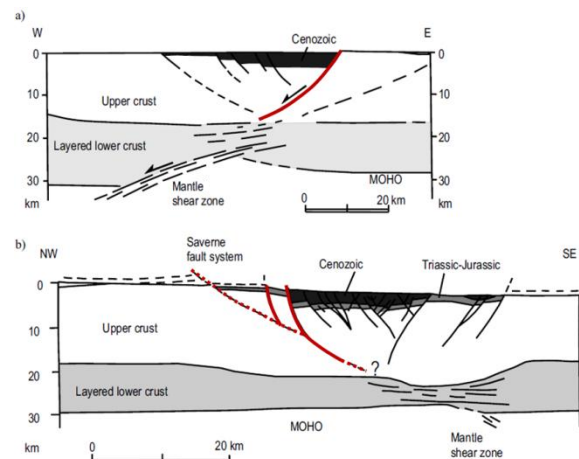
Recent thermo-tectono-stratigraphic forward modeling of the URG (Hinsken *et al.* 2010) suggests plane strain deformation perpendicular to the graben during the Middle Eocene to Early Miocene, Late Miocene post-rift stage and renewed rifting during the Pliocene to recent Rifting occurred at very low strain rate of about $1.7 \times 10^{-16} \, \text{s}^{-1}$ involving brittle-elastic deformation of the crust and ductile deformation of the highly viscous, high strength upper mantle and a 'pre-rift' necking depth of 29 km coinciding with the Moho. This is in agreement with previous results indicating a factor of extension of on average 1.15-1.2 for the whole rift and a total amount of E-W extension of 6-7 km during approximately 40 Ma (Villemin *et al.* 1986; Brun *et al.* 1992).

Today the URG boundary faults are thought to operate in a left lateral strike slip sense under the NW–SE oriented compression (Illies and Greiner 1979; Plenefisch and Bonjer 1997; Lopes Cardozo and Behrmann 2006) observed over much of Western Europe.

The URG is characterized by different asymmetries in the distribution of deformation (Fig. 1 and Fig. 2):
1. In the southern part, the sediment deposition center is located on the western side of the Graben (Brun *et al.* 1991), where the vertical motion (around 3 km) was accommodated by the western border fault (Brun *et al.* 1991; Cornu and Bertrand 2005)
2. In the northern part, the sediment deposition center is located on the eastern side of the graben where the vertical motion is maximum along the eastern border fault (Wenzel *et al.* 1991).
3. The master fault is interpreted to switch side in the southern transfer zone located at in the central part of the URG (Mauthe *et al.* 1993) (Fig. 1).

Graben wide seismic sections reveal fault zones down to a depth of 10-15 km (Fig. 2).

SHORT REVIEW OF GEODYNAMIC MODELING OF CONTINENTAL EXTENSION

Recent geodynamic modeling aims at predicting observations in rifting environments such as the geometry and modes of crustal extension (Huismans and Beaumont 2003; Huismans *et al.* 2005; Wijns *et al.* 2005; Buiter *et al.* 2008), the fault and strain distribution (Lavier *et al.* 2000; Regenauer-Lieb *et al.* 2008) and the distribution of continental strength in general. Major interests with respect to our study are:

1. What are the effects of extension and compression, and phenomena such as structural inheritance, basin inversion, and far-field stresses on the formation and evolution of sedimentary basins in extensional, compressional, and strike-slip settings?
2. How can we define the structural styles of faulting in the shallow brittle part of the lithosphere, the brittle–ductile transition, and the shear zone in the ductile part of the lithosphere?

On a global geological point of view rifting is firstly controlled by forces controlling the movement and interaction of lithospheric plates such as boundary stresses, slab pull, ridge push, collisional resistance, frictional forces caused mainly by the influence of the convecting mantle on the base of the lithosphere (Cloetingh *et al.* 2007). Cloetingh *et al.* (2007) argue, by looking at the best documented sedimentary basin systems in Europe (including the Upper Rhine graben), that the thermal and mechanical structure of the lithosphere is the main control on the development of sedimentary basins.

By considering direct evidence for fault strength, Scholz & Gerald (2007) conclude that stress in the lithosphere is limited by faulting and is determined, to first-order, by Byerlee's law with hydrostatic pressure (Watts and Gerald 2007). Byerlee's law describes the stress state in the Earth's upper crust at which fracturing along a geological fault takes place by solving the Mohr-Coulomb criterion:

$$\tau = Co + \mu \, (\sigma_n - Pf)$$

In which τ is the shear stress and σ_n the normal stress. Co is the cohesion or internal strength of the material and the value Pf is the pore fluid pressure inside the rock. The fact that pore pressure is hydrostatic in the crystalline rocks of the crust is a consequence of the high permeability of the crust resulting from the presence of faults (Townend and Zoback 2000; Scholz and Gerald 2007).

The geometry of rifts and sedimentary basins and their mode of extension are found to be linked to the amount of strain softening (the relation which describes the decrease of strength of a rock when subject to faulting) in the brittle upper crust, the thickness of the upper crust, the viscosity and strength of the lower crust, the extension rate and other processes linked with the extension such as gravitationally driven deformation, isostasy, magmatism and necking (Buiter *et al.* 2008) (and

references therein). They also analyzed the dependence of modes of crustal extension of a brittle crust on the strength of a ductile lower crust, its effective viscosity, the extension rate, and the layer thicknesses. They showed that an asymmetric basin is more likely to develop for a strong brittle layer which has a high amount of strain softening, a weak viscous layer (lower crust) and slow extension.

I- 2D CRUSTAL EXTENSION OF THE UPPER RHINE GRABEN AND IMPLICATION FOR GEOTHERMAL PROSPECTION

The aim of the study is to model the crustal extension of the Upper Rhine Graben satisfying the geophysical and geological observations in Fig. 2 and Fig. 3 with a localization of strain at one side of the Graben, in form of concentration of fault zones.

We use the geodynamic platform Underworld. It uses a Lagrangian *particle-in-cell* finite element scheme (Moresi *et al.* 2007) that enables the accurate tracking of stress and strain-rate history in simulations involving large-scale deformation. This platform includes a toolkit for studying the geodynamics of a viscoelastic-plastic lithosphere in 3D. This methodology has proven to be successful in simulating plausible scenarios for the creation of rifting environments such as the *distributed faulting mode* at the North Sea or *metamorphic core complexes* of the western U.S.A. and the Aegean (Wijns *et al.* 2005).

Sensitivity Study

We tested the effect of the initial settings on the faulting style during the extension, adapting input parameters from the model of Buiter *et al.* (2008) to values recorded in the URG (Figure 3 and Table 1).

We used a 2D two-layer model with an upper and a lower crust layer with the same uniform density. The upper crust deforms in a rigid-plastic manner using a Drucker-Prager frictional-plastic pressure dependent law which is an attempt to produce a smooth yield surface with otherwise similar characteristics to the Mohr–Coulomb yield surface (Moresi *et al.* 2007). There is an air layer above the solid material to approximate a free surface and allow the formation of topography. The sidewall boundary condition is free-slip vertically, with velocity conditions applied to the left and right to drive extension. An initial 100% damaged singularity was set at the boundary between the lower and upper crust to have control on the localization of the deformation.

Effect of a variation in viscosity

For this exercise, three models were stretched to reach 10% of deformation (5km on each side). The initial 100% damaged singularity was chosen to be 2x2 km. The lower crust viscosity values are 10^{21},

$5x10^{21}$ and 10^{22} Pa s are chosen in order to model the strength of an intermediately strong to a strong lower crust (Wijns *et al.* 2005).
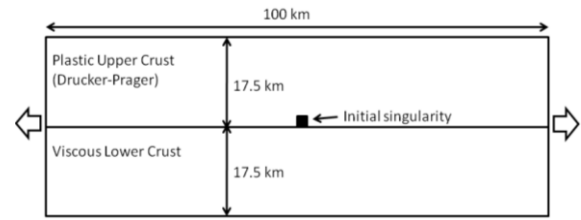

Figure 3: Model setup with plastic upper crust (Drucker-Prager frictional plastic pressure dependent law) and with viscous lower crust and an initial singularity

Table 1: Rheological and modeling parameters used during the presented crustal extension modeling.

Parameter	Natural Value	Unit
Thicknesses		
Crust	35	km
Brittle crust	17.5	km
Viscous crust	17.5	km
Width of the model	100	km
Extension velocity (per side)	$2,19x10^{-2}$*	cm.a^{-1}
Density Crust	2800	kg.m^{-3}
Angle of internal friction	30 -> 4	°
Cohesion	20 -> 2	MPa
Strain softening range	0-1	-
Linear viscosity (η)	10^{21} to 10^{22}	Pa.s

* The chosen value of extension velocity corresponds to a total amount 7km of graben extension over a 100km model during 40Ma (Villemin et al. 1986; Brun et al. 1992). This corresponds to a slow extension process (Hinsken et al. 2010).

The results are shown in Figure 4, represented in the final Lagrangian particle swarm distribution and cumulative strain rate distribution after 10 km of extension when using a lower crust viscosity of 10^{21} Pa s. As expected the singularity leads the deformation. A single fault crossing the entire upper crust appears during the first kilometers of extension when the lower crust strength is intermediate (Figure 4A) to intermediately high (Figure 4B). The deformation then starts to be distributed along a generation of normal and conjugate faults which forms the landscape of an asymmetric basin. The modeling of continental extension with an intermediately strong lower crust (Figure 4B) shows the apparition of an extra border fault on the other side of the graben and a relatively equal distribution of conjugate normal faults between the two border
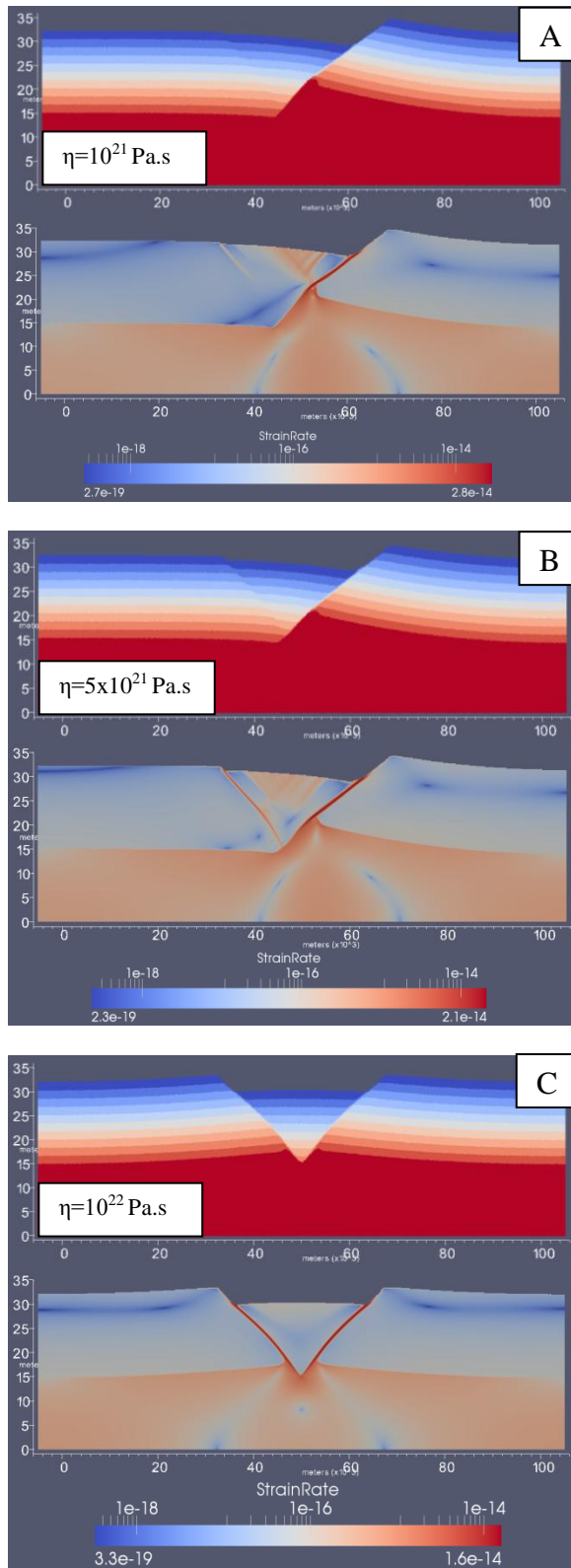
Figure 4(left):   Final Lagrangian particle swarm distribution (in km) (upper picture) and cumulative strain rate distribution (s-1) (lower picture) after 10 km of extension using a lower crust viscosity of A) 10^{21} Pa s, B) $5 \cdot 10^{21}$ Pa s, C) 10^{22} Pa s

faults. The presence of such faults are suggested in the crustal-scale seismic exploration of the Rhine Graben (Brun *et al.* 1992) but not yet clearly observed. Here, the effect of an initial singularity is probably too strong to see how the faults "naturally" develop. In the case where the lower crust is strong (Figure 4C), a symmetric basin tends to develop.

Effect of the initial geometry

In this part, the initial singularity was removed and replaced by a random distribution of damage within the envelope function $\varphi = sin^2 (k1. x1)$, where $k1 = 1/L1$ and *L1* is the length of the model, allowing the damage to be kept away from the boundaries (Figure 5).
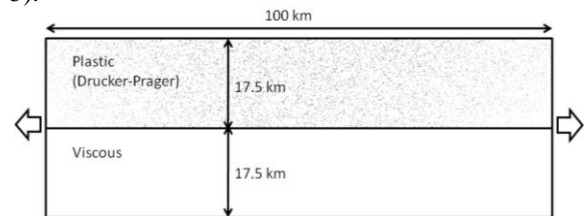

Figure 5:   Model setup. Grey dots represent the distribution (5%) of initially damaged material.

Three models were stretched to reach 15% of deformation as observed in the Upper Rhine graben (7.5 km on each side).

In the case of the low value of viscosity for the lower crust (i.e. intermediately strong lower crust), numerous faults develop in the early stages of the deformation in all model but they no longer accumulate slip after around 5% of extension and only one main fault take control over the deformation, stretching from the lower crust to the upper crust (Figure 6A). In the case of a stronger lower crust (i.e. viscosity values of $5x10^{21}$ and 10^{22} Pa s), in the two other models, this main fault is followed by the generation of conjugate faults at the surface. One of them (after 10% of extension) eventually grows and connects to the first main fault at the border between the two crusts, forming the second border fault of the basin (Figure 6B and C) Faults that are outside the basin tend to no longer accumulate slip, whereas the one that are inside the basin keep their shape and form the landscape of a graben and horst system mainly located on the side of the second border fault.

Another model with a lower crust viscosity value of 10^{23} Pa s was run: the resulting model shows the formation of multiple basins as we could expect for this high value (Buiter *et al.* 2008). This result is not comparable to what we observe in the URG.
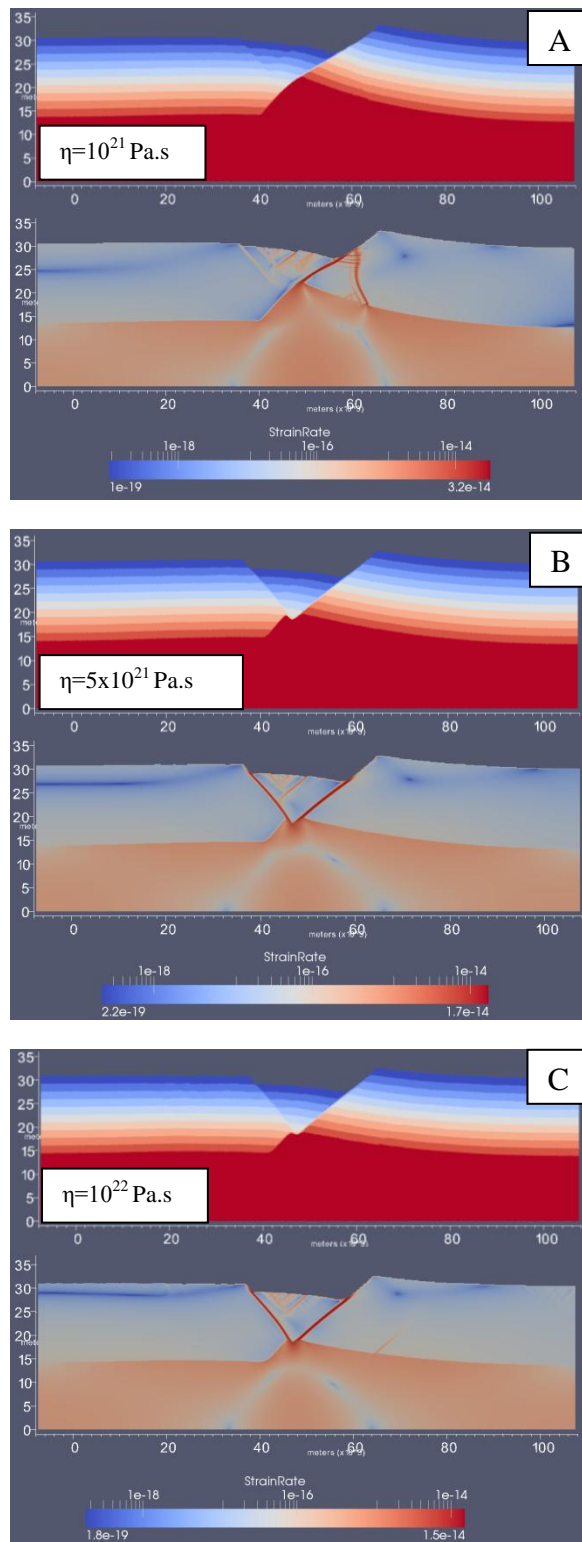
Figure 6: Final Lagrangian particle swarm distribution (in km) (upper picture) and cumulative strain rate distribution (s-1) (lower picture) after 15 km of extension using a lower crust viscosity of A) 10^{21} Pa s, B) $5·10^{21}$ Pa s, C) 10^{22} Pa s.

Comparison with independent geophysical data

The results of our geodynamic modeling find similarities with both the ECORS-DEKORP crustal-scale seismic exploration of the URG and the recent 3D geological model of the Soultz area, located at the western side in the central part of the URG:

For an intermediately strong to a strong lower crust, we find that after development of symmetrically conjugated faults, a preferential orientation develops into one main fault crossing the entire upper crust, which accommodates the deformation in this phase of graben formation. The presence of such a fault is suggested in the crustal-scale seismic exploration of the Rhine Graben (Brun *et al.* 1992). In the following phase a second boundary fault appears and the minor fault density is increasing in the area next to that boundary fault. This second boundary fault is also observed in the seismic results and provides indication for an asymmetric distribution of fault zones within a larger tectonic unit. This may explain also the fault density and temperature distribution in the area of Soultz.

Discussion and implication for geothermal exploration

Although we used simple assumptions (constant extension rate, no isostatic compensation, no shear heating, no temperature profile, no sediment deposition, no elasticity) to model the crustal extension, we find first order results that can be compared to geophysical data. For lower crust viscosity values of $5·10^{21}$ to 10^{22} Pa s, we approached the patterns of deformation observed in the Upper Rhine Graben.

These first order results have an implication for the geothermal prospection of the Cenozoic Europen Rift System. For example the supposed masterfaults could be potential for highly hydraulically conductive rocks as well as the region of horst and graben such as the Soultz area on the other side because of their long period of activity and renewed activity of the URG up to Recent.

II-GEOPHYSICAL RE-INTERPRETATION OF THE AREA OF SOULTZ

As temperature distributions, also other geophysical parameters reveal a number of anomalies throughout the investigation area. The focus of this study is the distribution of different anomalies with relation to the crystalline basement. To analyze the contribution of the basement to the temperature distribution, temperature data from the local 110 boreholes (Pribnow and Schellschmidt 2000) were interpolated in 3D and plotted on the basement top (Fig. 7).

Temperature highs are found to be not only located at the north-western part of the horst of Soultz but also about 7 km away in a south-east direction. In this area the top of the basement occurs at significant depth compared to Soultz. The distribution of faults however, shows a similar pattern.
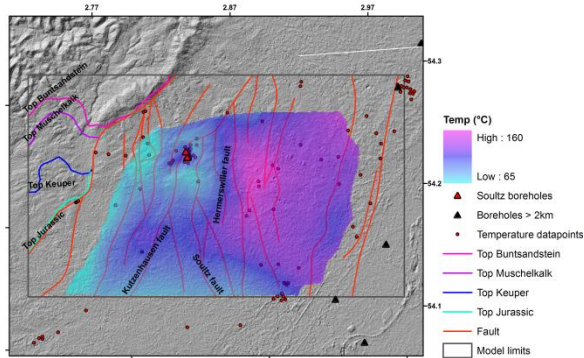

Figure 7: Temperature distribution on basement top. Fault and horizons traces are located on surface. Coordinates are in decimal degrees (UTM32N).

In order to investigate this apparent link between the structural pattern and the temperature distribution we used the high-resolution 3D structural regional model of the Soultz area (30x20x6km) (Fig. 8 and location in Fig. 1) as a basis for new geophysical reinterpretation and inversion of gravimetric and magnetic data anomalies.

Figure 8: 3D structural model of the Soultz area including the basement (grey), the Triassic-Jurassic layers (pink, purple, light and dark blue) and the fault planes (red). After (Baillieux et al. 2011).

To avoid physical inconsistency only a selection of the existing data from Rotstein *et al.* (2006) has been used in this study. The Bouguer anomaly (Fig. 9) shows an important gravity low in the region of Soultz, which has been attributed to a low density granitic and granodioritic basement of Lower Carboniferous age (Edel 2004). It occurs as several types of granite and sub-facies in the geothermal wells (Genter 1990; Hooijkaas *et al.* 2006) and reveals a characteristic density of 2630 kg m^{-3} (Rotstein *et al.* 2006) with local minima of down to 2460 kg m^{-3} in the hydrothermally altered zones with

a high clay content and a porosity of up to 20% (Genter 1990). Measurement on rock samples from the deeper levels resulted in a density of 2520 kg m^{-3} for the two-micagranite at 4909-4973 m and 2530 kg m^{-3} at 5018-5036 m for the biotite-rich granite in GPK3 borehole (Grecksch *et al.* 2003).
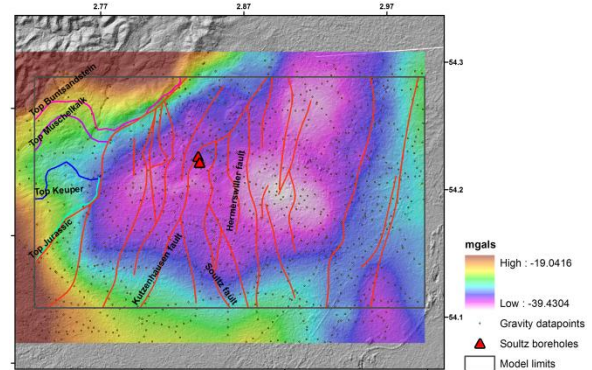

Figure 9: Bouguer Anomalies (in mgal) in the Soultz area. Coordinates are in decimal degrees (UTM32N).

In the central URG, the magnetic anomalies are attributed to pre-Permian basement bodies with different magnetic susceptibilities (Lauer and Taktak 1971; Edel *et al.* 1986; Edel and Fluck 1989). In the area of Soultz (Fig. 10), at the south-eastern side of the geothermal wells the 15 km-large magnetic structure has been estimated from surface magnetic measurements to be between 1.2 km and 2 km depth using half-slope methods (Papillon 1995), which corresponds to the depth of the top basement and to the measurements in the Soultz well. For example, in EPS1 borehole, the large increase in magnetic susceptibility in the granite was measured at 1550 km bsl (Rummel and König 1991) on granitic samples, below the Variscan paleo-surface. In other parts of the graben magnetic structures globally coincide as well with the lower Triassic depth, i.e. the top of the basement (Papillon 1995). Magnetic data of the URG and rock susceptibility measurements from the same areas showed generally that the magnetic bodies in the URG mostly correspond to Carboniferous gabbros, diorites and granodiorites, and their volcanic equivalents (Edel *et al.* 2006).

In the following, we compared the magnetic anomalies reduced to the pole (Fig. 10) with the tectonic features of our 3D geological model. In the central part of the model, it can be observed that the fault system follows the 15 km-large magnetic structure. Thus, this magnetic structure seems to have generated the localization of deformation during the graben opening.
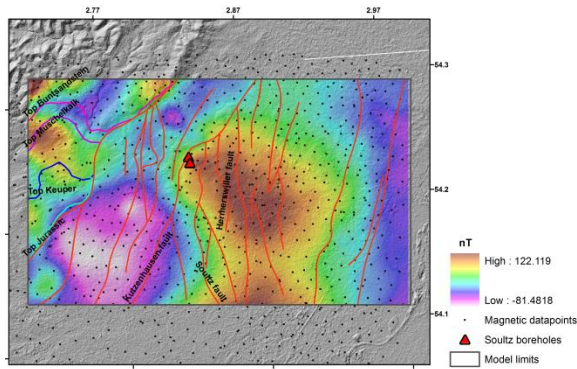
Figure 10: Magnetic anomalies reduced to the pole in the Soultz area (in mgal). Coordinates are in decimal degrees (UTM32N).

Inversion of the gravity data

Two 3D forward models with varying densities for the basement were calculated using GraviFor3D (Abdelfettah and Schill subm.) to investigate the gravimetric response of the geological model. Densities were chosen using values estimated in the URG (Plaumann 1967; Rousset *et al.* 1993; Rotstein *et al.* 2006) and measurements in the Soultz boreholes (Genter 1990) as well as from core samples (Rummel and König 1991).

Table 2: Densities of formations chosen for a forward modeling of the Bouguer anomaly at Soultz area.

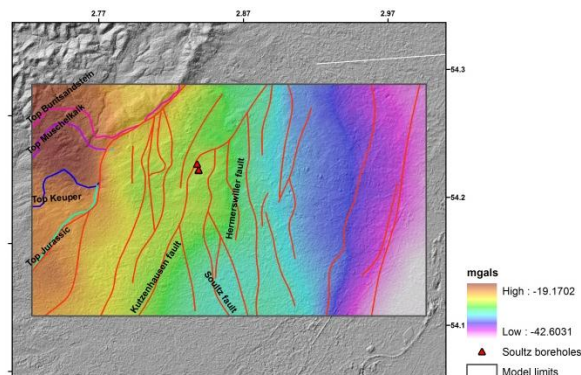| Formations	Density (kg m^{-3})
Tertiary	2350
Jurassic	2550
Keuper	2700
Muschelkalk	2700
Buntsandstein	2500
Basement	2500 (Fig. 11) 2600 (Fig. 12)

Figure 11: Forward modeling of the Bouguer anomaly at Soultz area with a uniform basement density of 2600 kg m^{-3}. Coordinates are in decimal degrees (UTM32N).
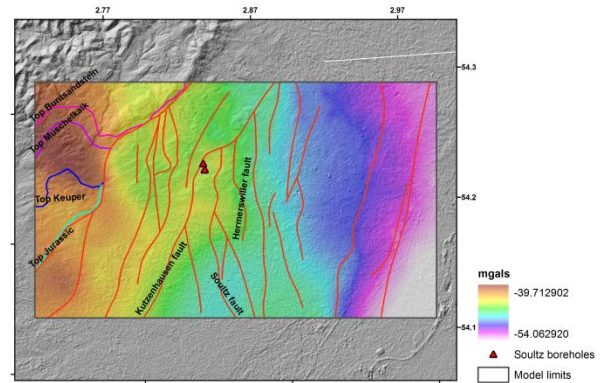

Figure 12: Forward modeling of the Bouguer anomaly at Soultz area with a uniform basement density of 2500 kg m^{-3}. Coordinates are in decimal degrees (UTM32N).

The first forward model with a basement density of 2600 kg m^{-3} fits the dynamic of the measurements (22 mgal in the forward model compared to 20 mgal in the Bouguer), but it is not in line with the observed anomalies (Fig. 11). The second forward model with a basement density of 2500 kg m^{-3} shows a dynamic by 12 mgal lower than the measured Bouguer anomalies (Fig. 12).

To match the dynamic of the forward modeling, we have applied a Butterworth 30 km high-pass filter to the measured Bouguer anomaly (Fig. 13). It results in a good fit in dynamic and density distribution with the results from the forward modeling with a uniform basement density of 2500 kg m^{-3}.
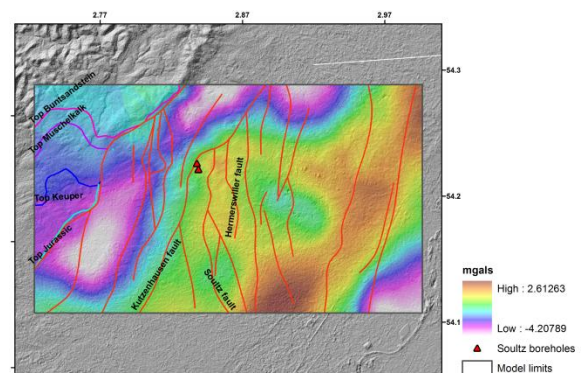

Figure 13: Residuals of the Bouguer Anomalies after Butterworth 30 km high-pass filter (in mgal) in the Soultz area. Coordinates are in decimal degrees (UTM32N).

Following this results we used the residual anomaly in Fig. 13 for inversion to determine densities that would fit the measurements. Gravity inversion can be considered as a linear or nonlinear approach. In the

first case, the objective is to find (invert) only the density values and geometries are considered as known. In the second case, the geometries and the densities are simultaneously inverted. The challenge of the inversion, especially for the potential method, is the non-uniqueness of the solution caused by the fact that the data number is always less than the parameters number used in the inversion run. For all these considerations, we chose to use the constrained 3D inversion in which the 3D geological model is fixed.

The minimization algorithm used is the routine developed by Beiner (1970). Principle of the inversion process is to minimize the misfit between the observed gravity data and the gravity response of the geological model. At each iteration, the forward modeling is achieved and its response is compared with real data and the discrepancy is minimized. As long as the misfit is great, the inversion parameters, the density values, are modified until that the minimization conditions are satisfied. This approach can be assimilated to a topographical surface in which we search the lowest elevation point (Fischer and Lequang 1981). The misfit function F is defined by

$$F(d) = \sum_{i=1}^{M} \left(\frac{g_i^{obs} - g_i^{com}}{\sigma_i} \right)^2 \qquad (1)$$

where d is the density or density contrast values, σ is the standard deviation of the observed data, g^{obs} and g^{com} are the observed and computed gravity anomalies, respectively. M is the total gravity measurements. The smoothness term of form

$$S(d) = \sum_{i=1}^{M} \sum_{j=i+1}^{M} [d(i) - d(j)]^2 \qquad (2)$$

can be added to the minimization defined in (1). This smoothness term is used to avoid a huge density contrast which may not be natural.

The results of the inversion are the densities determined in Table 3. The density values match the ones found in the literature. The basement density is found to be lower than expected. The gravimetric response of the model computed after inversion (Fig. 14) shows strong similarities with the residual anomaly, but also areas with important differences of up to 7 mgal (Fig. 15).

Table 3:   Densities determined by inversion.

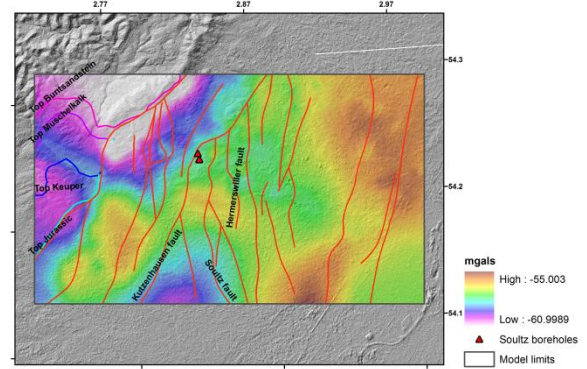| Formations	Initial density (g.cm^{-3})	After inversion (g.cm^{-3})
Tertiary	2.35	2.43 (+3.4%)
Jurassic	2.55	2.61 (+2.35%)
Keuper	2.7	2.58 (-4.4%)
Muschelkalk	2.7	2.64 (-2.2%)
Buntsandstein	2.5	2.66 (+6.4%)
Basement	2.5	2.41 (-3.6%)

Figure 14: Gravimetric response of the model computed after inversion (in mgal) in the Soultz area. Coordinates are in decimal degrees (UTM32N).
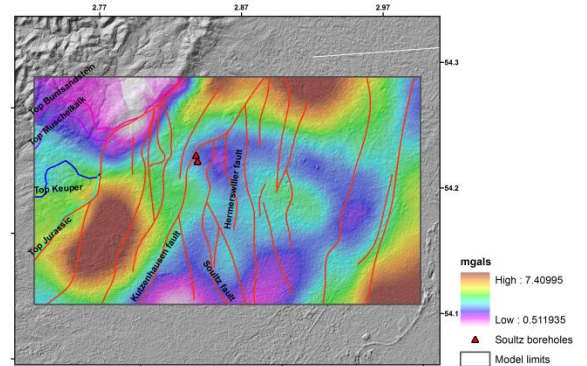

Figure 15: Difference between the gravimetric response of the model computed after inversion and the residuals (in mgal). Coordinates are in decimal degrees (UTM32N).

Interpretation

We find that the 3D geological model can explain most of the residual anomalies, if we use a low density value for the basement. The low density for the basement could be explained by a strong natural fracturing or/and the low density of the two-mica and biotite-rich granites that are found at depth in Soultz boreholes. The residuals also show zones of density lows that cannot be explained by the 3D model as demonstrated by the misfit. Interesting to note is that

about 1 mgal of misfit is observed in the area where the temperature distribution reveals a positive anomaly. As observed in Soultz such temperature anomalies go along with porosity anomalies. For example, for the reservoir zones of Soultz, we observe a mean porosity of about 8%.

Within the horst structure of the Soultz site, a density difference can be observed between the eastern and the western part. In the West, the residual anomaly is slightly smaller compared to the East. This, combined with the magnetic anomaly present at that location gives us interesting information: the Kutzenhausen-Soultz fault zone is a major structure in the region and has probably a large influence on the state of fracturing at Soultz.

CONCLUSION

The geodynamic approach we used provides insights in the localization of permeable structures at a regional level, at a first order comparable to the patterns of deformation observed in the Upper Rhine Graben.

The processing and inversion of gravity, the magnetic and temperature measurements and the 3D geological model reveal certain correlations at a local level, such as distribution of low density areas correlated to geothermal positive anomalies. The basement was found to be of a lower density than expected. This is in favor of a naturally porosity or low density basement lithology.

ACKNOWLEDGEMENTS

REFERENCES

Abdelfettah, Y. and E. Schill (subm.). 'GraviFor3D: Accurate gravity data correction and 3D forward modeling Fortran code'. Computers & Geosciences.

Bachler, D., T. Kohl, et al. (2003). 'Impact of graben-parallel faults on hydrothermal convection - Rhine Graben case study'. Physics and Chemistry of the Earth 28(9-11): 431-441.

Baillieux, P., E. Schill, et al. (2011). '3D structural regional model of the EGS Soultz site (northern Upper Rhine Graben, France): insights and perspectives'. PROCEEDINGS, Thirty-Sixth Workshop on Geothermal Reservoir Engineering, Stanford University, Stanford, California, SGP-TR-191.

Beiner, J. (1970). 'Fortran routine mindef for function minimization'. Institut de Physique, Univ. of Neuchatel, Switzerland(65): 1-13.

Brun, J. P., M. A. Gutscher, et al. (1992). 'Deep crustal structure of the Rhine Graben from seismic reflection data: A summary'. Tectonophysics 208(1-3): 139-147.

Brun, J. P., F. Wenzel, et al. (1991). 'Crustal-scale structure of the southern Rhinegraben from ECORS-DEKORP seismic reflection data'. Geology 19: 758--762.

Buiter, S. J. H., R. S. Huismans, et al. (2008). 'Dissipation analysis as a guide to mode selection during crustal extension and implications for the styles of sedimentary basins'. Journal of Geophysical Research-Solid Earth 113(B6): -.

Cloetingh, S., J. D. van Wees, et al. (2010). 'Lithosphere tectonics and thermo-mechanical properties: An integrated modelling approach for Enhanced Geothermal Systems exploration in Europe'. Earth-Science Reviews 102(3-4): 159-206.

Cloetingh, S., P. A. Ziegler, et al. (2007). Tectonic Models for the Evolution of Sedimentary Basins. Treatise on Geophysics. Amsterdam, Elsevier: 485-611.

Cornu, T. G. M. and G. Bertrand (2005). 'Numerical backward and forward modelling of the southern Upper Rhine Graben (France-Germany border): new insights on tectonic evolution of intracontinental rifts'. Quaternary Science Reviews 24(3-4): 353-361.

Derer, C. E., M. E. Schumacher, et al. (2005). 'The northern Upper Rhine Graben: basin geometry and early syn-rift tectono-sedimentary evolution'. 640-656.

Dèzes, P., S. M. Schmid, et al. (2004). 'Evolution of the European Cenozoic Rift System: interaction of the Alpine and Pyrenean orogens with their foreland lithosphere'. Tectonophysics 389: 1--33.

Edel, J. B. (2004). 'Structure et évolution du Fossé Rhénan, du Carbonifère à nos jours - apports de la géophysique'. Bulletin de la société d'histoire naturelle et d'éthnographie de Colmar 65(2004): 21-50.

Edel, J. B. and P. Fluck (1989). 'The Upper Rhenish Shield Basement (Vosges, Upper Rhinegraben and Schwarzwald) - Main Structural Features Deduced from Magnetic, Gravimetric and Geological Data'. Tectonophysics 169(4): 303-316.

Edel, J. B., R. Montigny, et al. (1986). 'Paleomagnetic investigations and K-AR dating on the variscan plutonic massif of the champ du feu and its volcanic-sedimentary environment, northern vosges, France'. Tectonophysics 122(1-2): 165-185.

Edel, J. B., K. Schulmann, et al. (2006). 'The Variscan tectonic inheritance of the Upper Rhine Graben: evidence of reactivations in the Lias, Late Eocene-Oligocene up to the recent'. International Journal of Earth Sciences.

Edel, J. B., K. Schulmann, et al. (2006). 'The Variscan tectonic inheritance of the Upper Rhine Graben: evidence of reactivations in the Lias, Late Eocene-Oligocene up to the recent'. International Journal of Earth Sciences 96(2): 305-325.

Fischer, G. and B. V. Lequang (1981). 'Topography and Minimization of the Standard-Deviation in One-Dimensional Magnetotelluric Modeling'. Geophysical Journal of the Royal Astronomical Society 67(2): 279-292.

Geiermann, J. and E. Schill (2010). '2-D Magnetotellurics at the geothermal site at Soultz-sous-Forets: Resistivity distribution to about 3000 m depth'. Comptes Rendus Geoscience 342(7-8): 587-599.

Genter, A. (1990). Géothermie roches chaudes sèches: le granite de Soultz-sous-Forêts. (Bas-Rhin, France), Fracturation naturelle, altérations hydrothermales et interaction eau-roche, Université d'Orléans. **PhD:** 201.

Genter, A., H. Traineau, et al. (1995). 'Fracture analysis and reservoir characterization of the granitic basement in the HDR Soultz project (France)'. Geothermal Science and Technology 4(3): 189-214.

Grecksch, G., A. Ortiz, et al. (2003). 'Thermophysical Study of GPK2 and GPK3

Granite Samples'. HDR Project Soultz - Report.

Hinsken, S., S. M. Schmalholz, et al. (2010). 'Thermo-Tectono-Stratigraphic Forward Modeling of the Upper Rhine Graben in reference to geometric balancing: Brittle crustal extension on a highly viscous mantle'. Tectonophysics In Press, Accepted Manuscript.

Hooijkaas, G. R., A. Genter, et al. (2006). 'Deep-seated geology of the granite intrusions at the Soultz EGS site based on data from 5 km-deep boreholes'. Geothermics 35(5-6): 484-506.

Huismans, R. S. and C. Beaumont (2003). 'Symmetric and asymmetric lithospheric extension: Relative effects of frictional-plastic and viscous strain softening'. J. Geophys. Res. 108(B10): 2496.

Huismans, R. S., S. J. H. Buiter, et al. (2005). 'Effect of plastic-viscous layering and strain softening on mode selection during lithospheric extension'. J. Geophys. Res. 110(B2): B02406.

Illies, H. J. and G. Greiner (1979). 'Holocene movements and state of stress in the rhinegraben rift system'. Tectonophysics 52(1-4): 349--359.

Illies, J. H. (1965). 'Bauplan und Baugeschichte des Oberrheingrabens. Ein Beitrag zum "Upper Mantle Project"'. Oberrheinische Geologische Abhandlungen 14: 1-54.

Kohl, T., D. Bächler, et al. (2000). 'Steps towards a comprehensive thermo-hydraulic analysis of the HDR test site Soultz-sous- Forêts.'. Proc. World Geothermal Congress 2000, Kyushu-Tohoku, Japan, May–June 2000, pp. 2671–2676.

Lauer, J. P. and A. G. Taktak (1971). 'Propriétés magnétiques des roches au voisinage du contact métamorphique des schistes de Steige et des granites d'Andlau et du Hohwald (Vosges cristallines du Nord)'. C.R. Acad. Sci., Paris 272, 924-927.

Lavier, L. L., W. R. Buck, et al. (2000). 'Factors controlling normal fault offset in an ideal brittle layer'. Journal of Geophysical Research-Solid Earth 105(B10): 23431-23442.

Lopes Cardozo, G. G. O. and J. H. Behrmann (2006). 'Kinematic analysis of the Upper Rhine Graben boundary fault system'. Journal of Structural Geology 28(6): 1028-1039.

Mauthe, G., H.-J. Brink, et al. (1993). 'Kohlenwasserstoffvorkommen und -potential im deutschen Teil des Oberrheingrabens'. 60.

Moresi, L., H.-B. MÃ¼hlhaus, et al. (2007). 'Incompressible viscous formulations for deformation and yielding of the lithosphere'. Geological Society, London, Special Publications 282(1): 457-472.

Moresi, L., S. Quenette, et al. (2007). 'Computational approaches to studying non-linear dynamics of the crust and mantle'. Physics of The Earth and Planetary Interiors 163(1-4): 69-82.

Papillon, E. (1995). 'Traitements et interpretations des cartes d'anomalies magnétiques et gravimétriques du Fossé Rhénan supérieur'. Dipl. Ing. Géophs. Strasbourg I, 95p.

Plaumann, P. (1967). 'Erweiterungen Kompakter Gruppen Durch Abelsche Gruppen'. Mathematische Zeitschrift 99(2): 123-&.

Plenefisch, T. and K. P. Bonjer (1997). 'The stress field in the Rhine Graben area inferred from earthquake focal mechanisms and estimation of frictional parameters'. Tectonophysics 275(1-3): 71-97.

Pribnow, D. and R. Schellschmidt (2000). 'Thermal tracking of upper crustal fluid flow in the Rhine Graben'. Geophysical Research Letters 27(13): 1957-1960.

Regenauer-Lieb, K., G. Rosenbaum, et al. (2008). 'Strain localisation and weakening of the lithosphere during extension'. Tectonophysics 458(1-4): 96-104.

Rotstein, Y., J. B. Edel, et al. (2006). 'Insight into the structure of the Upper Rhine Graben and its basement from a new compilation of Bouguer Gravity'. Tectonophysics 425(1-4): 55-70.

Rousset, D., R. Bayer, et al. (1993). 'Structure of the Southern Rhine Graben from Gravity and Reflection Seismic Data (Ecors-Dekorp Program)'. Tectonophysics 221(2): 135-153.

Rummel, F. and E. König (1991). 'Density, ultrasonic velocities and magnetic susceptibility measurements on the core material from borehole EPS1 at Soultz-sous-Forêts.'. Yellow report 8(1991).

Schill, E., J. Geiermann, et al. (2010). '2-D Magnetotellurics and gravity at the geothermal site at Soultz-sous-Forêts'. Proceedings World Geothermal Congress 2010 Bali, Indonesia, 25-29 April 2010.

Scholz, C. H. and S. Gerald (2007). Fault Mechanics. Treatise on Geophysics. Amsterdam, Elsevier**:** 441-483.

Schumacher, M., E. (2002). 'Upper Rhine Graben: Role of preexisting structures during rift evolution'. Tectonics 21(1): 1006.

Townend, J. and M. D. Zoback (2000). 'How faulting keeps the crust strong'. Geology 28(5): 399-402.

Villemin, T., F. Alvarez, et al. (1986). 'The Rhinegraben: Extension, subsidence and shoulder uplift'. Tectonophysics 128(1-2): 47-59.

Villemin, T. and F. Bergerat (1987). 'L'évolution structurale du fossé rhénan au cours du Cénozoïque : un bilan de la déformation et des effets thermiques de l'extension.'. Bulletin de la Société Géologique de France 3(2): 245--255.

Watts, A. B. and S. Gerald (2007). An Overview. Treatise on Geophysics. Amsterdam, Elsevier**:** 1-48.

Wenzel, F., J.-p. Brun, et al. (1991). 'A deep seismic reflection profile across the northern rhine graben'.

Wijns, C., R. Weinberg, et al. (2005). 'Mode of crustal extension determined by rheological layering'. Earth and Planetary Science Letters 236(1-2): 120-134.

Ziegler, P. A. (1992). 'European Cenozoic rift system'. Tectonophysics 208(1-3): 91-111.